BIOCELL

Tech Science Press

http://doi.org/10.32604/biocell.2026.075362

ARTICLE

METTL3-Mediated m6A Regulation of PTEN Promotes Macrophage Ferroptosis in Gouty Arthritis

Gang Yang[#], Xiongwu Long[#] and Xingchang Fu[*]

Joint Surgery Department of Hunan Aerospace Hospital, No. 189, Fenglin 3rd Road, Changsha, China
*Corresponding Author: Xingchang Fu. Email: fuxingchang@gt.cn
#These authors contributed equally to this work as the first author

Received: 30 October 2025; Accepted: 12 February 2026; Published: 29 June 2026

ABSTRACT: Objectives: Macrophage ferroptosis is linked to the pathogenesis of gouty arthritis (GA), yet the precise regulatory mechanism needs to be elucidated. This study aimed to investigate the role of macrophage ferroptosis in GA and its potential mechanisms. **Methods:** THP-1 macrophages were stimulated with monosodium urate (MSU) crystals to simulate the GA model. The co-culture system of macrophages and primary chondrocytes (hCDs) was employed to analyze the effects of macrophage-mediated inflammation on chondrocyte degeneration. **Results:** MSU stimulation induced ferroptosis in macrophages, accompanied by increased methyltransferase-like 3 (METTL3) expression ($p = 0.003$) and total m6A modification level ($p = 0.0058$). In MSU-induced macrophages, phosphatase and tensin homolog (PTEN) knockdown activated the phosphoinositide 3-kinase (PI3K)/protein kinase B (AKT) pathway ($p < 0.0001$), downregulated glutathione peroxidase 4 (GPX4; $p = 0.0006$), solute carrier family 7 member 11 (SLC7A11; $p < 0.0001$), glutathione (GSH; $p = 0.0149$), and superoxide dismutase (SOD; $p = 0.0165$) levels, and enhanced lipid peroxidation, malondialdehyde (MDA; $p < 0.0001$), Fe^{2+} ($p < 0.0001$), and pro-inflammatory cytokines ($p < 0.01$). Additionally, PTEN knockdown in macrophages reduced the co-localization of GPX4 and cluster of differentiation 68 (CD68; $p < 0.0001$), promoting macrophage ferroptosis. Co-culture with PTEN-knockdown macrophages impaired hCD viability, elevating MMP3 ($p < 0.0001$) while reducing Collagen II ($p < 0.0001$) and Aggrecan ($p < 0.0001$). Mechanistically, METTL3 decreased PTEN mRNA stability ($p < 0.0001$) and gene expression by m6A modification. The m6A reader YT521-B homology domain family protein 2 (YTHDF2) interacted with PTEN ($p < 0.0001$). METTL3/YTHDF2-mediated PTEN led to activation of the PI3K/AKT pathway and promotion of ferroptosis and inflammation. **Conclusions:** METTL3/YTHDF2-mediated PTEN drives GA progression by modulating the PI3K/AKT pathway in macrophages, which induces ferroptosis and chondrocyte degeneration. Targeting METTL3-mediated m6A modification and PTEN may represent promising therapeutic strategies for arthritis.

KEYWORDS: Gouty arthritis; methyltransferase-like 3; phosphatase and tensin homolog; m6A modification; macrophage; ferroptosis

1 Introduction

Gouty arthritis (GA) is an inflammatory joint disorder triggered by the deposition of monosodium urate (MSU) crystals within articular structures, resulting in severe pain and swelling for patients [1]. The initial pathogenesis begins with MSU crystals activating joint-resident macrophages, which release pro-inflammatory mediators like interleukin-1 beta (IL-1β), IL-6, and tumor necrosis factor-alpha (TNF-α), thereby driving the acute attack and chondrocyte degeneration through the inhibition of matrix synthesis (Collagen II, Aggrecan) and upregulation of degradative enzymes like MMP3 [2,3]. Although first-line

Copyright © 2026 The Authors. Published by Tech Science Press. This work is licensed under a Creative Commons Attribution 4.0 International License, which permits unrestricted use, distribution, and reproduction in any medium, provided the original work is properly cited.

therapies like glucocorticoids, nonsteroidal anti-inflammatory drugs (NSAIDs), and colchicine effectively manage acute attacks, they exhibit substantial adverse effects [4]. Given the rising global prevalence of GA [5], elucidating its molecular mechanisms and identifying novel therapeutic targets are critical for improving clinical outcomes.

Ferroptosis is a programmed cell death pathway characterised fundamentally by iron-dependent lipid peroxidation, and is distinct from apoptosis and pyroptosis [6]. Studies have shown that excessive iron in synovial fluid correlates positively with the severity of rheumatoid arthritis [7]. Notably, while M2 macrophages are highly susceptible to ferroptosis, pro-inflammatory M1 macrophages are conversely more resistant [8]. The process of inhibiting macrophage ferroptosis has been demonstrated to promote anti-inflammatory M2 polarization, thus attenuating the progression of arthritis [8,9]. In GA, the dysfunction of macrophages, triggered by MSU crystals, has been identified as a pivotal factor in the progression of inflammation [10,11]. This process occurs in parallel with disrupted iron metabolism, which is characterised by abnormal iron accumulation. Such accumulation impairs uric acid homeostasis and further contributes to the pathogenesis of the disease [12,13]. Clinical evidence confirms positive correlations between elevated serum ferritin and iron levels and urate concentrations [14], suggesting ferroptosis-related pathways may serve as diagnostic and therapeutic biomarkers for GA [15]. Nevertheless, the precise role and regulatory mechanisms of macrophage ferroptosis in GA have yet to be fully elucidated.

The Phosphatase and Tensin Homolog (PTEN) gene, located at 10q23.3, functions as a tumor suppressor and directly modulates the phosphatidylinositide 3-kinases/protein kinase B (PI3K/AKT) pathway [16]. As a core regulator of cell proliferation and immune homeostasis, the PTEN/PI3K/AKT axis plays a significant role in GA pathogenesis [17,18]. From a mechanistic perspective, N6-methyladenosine (m6A) modification regulates PTEN expression by modulating the stability and translation efficiency of its mRNA [19,20]. This regulation, in turn, influences key cellular processes including inflammatory responses, mitochondrial function, and cell death [21,22]. Methyltransferase-like 3 (METTL3), a core catalytic enzyme for m6A modification, is highly expressed in macrophages and participates in regulating macrophage inflammatory responses and reactive oxygen species production [23,24]. Li et al.'s research demonstrated that inflammation and oxidative stress downregulate METTL3. This decrease reduces m6A modification, leading to the downregulation of insulin secretion-related genes [25]. Wu et al.'s research revealed that METTL3 inhibits ferroptosis in non-small cell lung cancer cells through the PTEN/PI3K/AKT pathway [26].

However, it remains unknown whether m6A modification of PTEN regulates macrophage ferroptosis in GA. Therefore, we aimed to investigate the molecular mechanism of the METTL3/PTEN axis in ferroptosis and GA pathogenesis. We hypothesized that METTL3-mediated PTEN m6A modification may promote ferroptosis in macrophages. To test this, we established an *in vitro* GA model by stimulating THP-1-derived macrophages using MSU and co-culturing the human primary chondrocytes (hCDs) for this investigation.

2 Methods and Materials

2.1 Preparation of Drugs

For the preparation of MSU crystals [27], 1 g of uric acid (U755689, Aladdin, Shanghai, China) and 0.5 g of sodium hydroxide (S774711, Aladdin) were dissolved in 100 mL of ddH_2O (Top1205S, Biotopped, Beijing, China) at room temperature. The solution was heated in an 80°C water bath for 20 min until clear. After cooling at 4°C overnight, the crystal was formed. Then the pH was adjusted to approximately 7.2 by titration with dilute hydrochloric acid to promote further crystal growth. The obtained precipitate was dried (70°C, 4 h), ground into a powder, and dry-heat sterilized (180°C, 2 h). Before administration, the MSU crystals were suspended in sterile PBS (pH 7.2–7.6; 0.01 mol/L) to prepare a 500 μg/mL solution. For phorbol

12-myristate 13-acetate (PMA; HY-18739, MCE, Monmouth Junction, NJ, USA) solution, we prepared a 1 mg/mL stock solution of PMA in DMSO. Subsequently, the stock solution was diluted 10,000-fold before application at a final concentration of 100 ng/mL.

2.2 Cell Culture and Treatment

Human primary chondrocytes (hCDs, AW-YCH026, Abiwell, Changsha, China) and acute monocytic leukemia cell line THP-1 (AW-CCH098, Abiowell, Changsha, China) were maintained in RPMI-1640 (R8758, Sigma, St. Louis, MO, USA) containing 10% fetal bovine serum (FBS; Gibco, Carlsbad, CA, USA; 10099141) and 1% penicillin/streptomycin (P/S; C0222, Beyotime, Shanghai, China) at 37°C in 5% CO_2. THP-1 cells were exposed to PMA solution (100 ng/mL) for 48 h to induce macrophages [27]. THP-1-derived macrophages were exposed to MSU (500 μg/mL) for 12 h to establish a GA model *in vitro* [28]. All cell lines used in this study have been authenticated and confirmed to be free of mycoplasma contamination. Cell line authentication and mycoplasma contamination testing reports are provided in Supplementary File S1.

To investigate the roles of PTEN/METTL3, we transfected differentiated THP-1 cells with plasmids overexpressing PTEN (oe-PTEN), overexpressing METTL3 (oe-METTL3), knocking down PTEN (sh-PTEN), and knocking down METTL3 (sh-METTL3) or corresponding negative controls (oe-NC or sh-NC) for 48 h. The transfection procedure is as follows: The transfection plasmid was thawed on ice. Two tubes received 95 μL of serum-free RPMI 1640 medium. Then, 3 μg of plasmid and 5 μL of Lipofectamine 2000 (11668019, Invitrogen, Carlsbad, CA, USA) reagent were added to the corresponding tubes, respectively. The mixed solution was added evenly. The details of the plasmids were as follows: sh-PTEN (HG-SH000314, Honorgene, Changsha, China), oe-PTEN (HG-HO000314, HonorGene), sh-METTL3 (HG-H019852, HonorGene), oe-METTL3 (HG-HO019852, HonorGene), sh-PTEN: 5′-GGGCTTTAACTGTAGTATTTG-3′, sh-METTL3: 5′-GCCTTAACATTGCCCACTGAT-3′, sh-NC: 5′-TTCTCCGAACGTGTCACGT-3′.

To explore the relationship between PTEN and ferroptosis, THP-1-derived macrophages were treated with Ferrostatin-1 (Fer-1; Concentration: 10 mM in DMSO, F408509; Aladdin; Shanghai, China). The cells were divided into the following groups: MSU-treated (500 μg/mL MSU); MSU-treated+Fer-1 (500 μg/mL MSU + 2 μM Fer-1); MSU+sh-NC (transfected with sh-NC, then treated with 500 μg/mL MSU); MSU+sh-PTEN (transfected with sh-PTEN, then treated with 500 μg/mL MSU); MSU+sh-PTEN+Fer-1 (transfected with sh-PTEN, then treated with 500 μg/mL MSU + 2 μM Fer-1). All treatments involving Fer-1 lasted for 24 h [8].

THP-1 cells were subjected to plasmid transfection and then stimulated with MSU, followed by co-culture with hCDs using a transwell system with a 0.4 μm pore size (723111, NEST, Wuxi, China). THP-1 and hCDs were seeded in the upper and lower chambers, respectively, at a density of 1.5×10^5 cells per well. The co-culture was maintained in RPMI-1640 medium supplemented with 10% FBS and 1% P/S, and incubated at 37°C with 5% CO_2 in a humidified incubator for 24 h [29].

2.3 Reverse Transcription Quantitative PCR (RT-qPCR)

Total RNA from hCDs or THP-1 cells was extracted with TRIzol reagent (15596026, Thermo Fisher Scientific, Waltham, MA, USA). cDNA was synthesized with 2 μg RNA employing a reverse transcription kit (CW2569, CWbio, Beijing, China). qPCR amplification was performed using a 20 μL reaction system comprising 10 μL of Ultra SYBR Mixture (CW2601, CWBio), 1 μL of corresponding primers (10 μM), 2 μL of cDNA, and nuclease-free water. The thermal profile consisted of 95°C for 10 min, followed by 40 cycles of 95°C (15 s) and 60°C (30 s), and then a melt curve ramp (65–95°C). Triplicate reactions were analyzed, and relative gene expression quantified via the $2^{-\Delta\Delta Ct}$ method with β-actin as the Control. Primer sequences are shown in Table 1.

Table 1: Primer sequences.

Name	Primer 5′–3′	Length
METTL3	Forward: ATATTCACATGGAACTGCCCTA Reverse: ATTTCATCTACCCGTTCATACCC	169 bp
PTEN	Forward: AATTGGCCGCTGTCACT Reverse: GCCCATTCTTTGTTGATAGCCT	225 bp
β-actin	Forward: ACCCTGAAGTACCCCATCGAG Reverse: AGCACAGCCTGGATAGCAAC	224 bp

2.4 Western Blot (WB)

Protein was isolated from hCDs or THP-1-derived macrophage cells using RIPA (AWB0136, Abiowell) and quantified with a BCA kit (AWB0104, Abiowell). After denaturation in loading buffer, proteins were separated by electrophoresis and transferred to nitrocellulose membranes. The membranes were blocked using 5% skimmed milk (P1622, Applygen, Beijing, China) for 1.5 h, followed by incubation with primary antibodies targeting PTEN, METTL3, p-PI3K, PI3K, p-AKT, AKT, GPX4, SLC7A11, MMP3, Collagen II, Aggrecan, or ALOX15 overnight at 4°C, with β-actin as the Control. Detailed antibody information is shown in Table 2. Subsequently, the membranes were incubated with the secondary antibody for 1.5 h. After incubation, membranes were washed three times, each for 15 min. ECL chromogenic substrate (AWB0005, Abiowell) was used to visualize protein bands. For scanning and imaging, chemiluminescence imaging (ChemiScope6100, Clinx, Shanghai, China) was used. WB band intensity was quantified using ImageJ software (version 1.53, National Institutes of Health, Bethesda, MD, USA). A single band confirmed specificity at the expected molecular weight in WB. The primary antibodies in the study are validated for reactivity with human and mouse proteins. This information was referenced from the manufacturer's website (Abcam: https://www.abcam.com; Proteintech: https://www.ptglab.com). The uncropped raw images of all WB bands are seen in Supplementary File S2.

Table 2: Antibodies used for WB in the study are shown.

Name	Dilution	Catalog Number	Source	Molecular Weight	Company
PTEN	1:1000	ab267787	Rabbit	54 kDa	Abcam
p-PI3K	1:1000	ab278545	Rabbit	84 kDa	Abcam
PI3K	1:1000	ab191606	Rabbit	84 kDa	Abcam
p-AKT	1:3000	28731-1-AP	Rabbit	58 kDa	Proteintech
AKT	1:6000	10176-2-AP	Rabbit	56–62 kDa	Proteintech
GPX4	1:1000	67763-1-Ig	Mouse	20–23 kDa	Proteintech
SLC7A11	1:1000	AWA00502	Mouse	55 kDa	Abiowell
METTL3	1:10,000	15073-1-AP	Rabbit	65–70 kDa	Proteintech
MMP3	1:10,000	ab52915	Rabbit	50 kDa	Abcam
Collagen II	1:1000	ab34712	Rabbit	141 kDa	Abcam
Aggrecan	1:1000	ab3778	Mouse	250 kDa	Abcam
ALOX15	1:1000	ab244205	Rabbit	75 kDa	Abcam
HRP goat anti-mouse IgG	1:5000	SA00001-1	Mouse	/	Proteintech
HRP goat anti-rabbit IgG	1:6000	SA00001-2	Rabbit	/	Proteintech
β-actin	1:5000	66009-1-Ig	Mouse	42 kDa	Proteintech

2.5 Immunofluorescence (IF)

A double-labeled immunofluorescence for GPX4 and CD68 was performed using a commercial kit (AWI0693a, Abiowell). THP-1-derived macrophages were seeded on sections and fixed in 4% paraformaldehyde

for 30 min, then permeabilized and blocked with 0.3% Triton X-100 and 3% H_2O_2. After blocking with 5% BSA in phosphate buffer (pH 7.2–7.6; 0.01 mol/L), the sections were incubated overnight at 4°C with appropriately diluted primary antibodies against GPX4 (AWA11352, 1:50, Abiowell, validated for IF application) and CD68 (AWA58061, 1:50, Abiowell, validated for IF application). Following three washes with PBS (5 min each), the sections were incubated with 50 μL of HRP-conjugated secondary antibody (HRP goat anti-mouse IgG, AWS0001-1, dilution ratio = 1:5000, Proteintech, Chicago, IL, USA; HRP goat anti-rabbit IgG, SA00001-2, dilution ratio = 1:5000, Proteintech, validated for IF application). Specificity was confirmed by appropriate subcellular localization in IF. Subsequently, the nuclei were counterstained with DAPI solution (5 μg/mL; AWC0293a, Abiowell) at 37°C for 10 min. After a final series of washes with PBS, sections were mounted with buffered glycerol and imaged using a fluorescence microscope (BA210T, Motic, Xiamen, China).

2.6 Cell Counting Kit-8 (CCK8)

The hCDs (3×10^4) were inoculated into 24-well plates and treated with 30 μL of CCK8 (AWC0114a, Abiowell) solution in mixed medium. Following a 4-h incubation, samples were subjected to an OD measurement at 450 nm using a microplate reader (MB-530, Huisong, China).

2.7 RNA Stability

To assess PTEN mRNA stability, transcription was inhibited by treating THP-1-derived macrophages with actinomycin D (2 μM; A432787, Aladdin). Cells were collected at 0, 6, and 12 h after termination. The total RNA was isolated, and RT-qPCR was used to determine the PTEN mRNA level.

2.8 Biochemical Kit Detection

After THP-1-derived macrophage cells were lysed, Fe^{2+} content kit (JL-T1255, JONLNBIO, Shanghai, China), glutathione (GSH) kit (A006-2-1, Nanjing Jiancheng Bioengineering Institute, China), malondialdehyde (MDA) Kit (A003-1-2, Nanjing Jiancheng Bioengineering Institute), m6A RNA Methylation Quantification Kit (Ab185912, Abcam, Cambridge, UK), and superoxide dismutase (SOD) kit (A001-3, Nanjing Jiancheng Bioengineering Institute) were utilized to detect Fe^{2+}, GSH, MDA, total m6A and SOD levels.

2.9 Enzyme-Linked Immunosorbent Assay (ELISA)

The concentration of IL-1β (CSB-E04740h, Cusabio, Wuhan, China), IL-6 (CSB-E04638h, Cusabio), and TNF-α (CSB-E08053h, Cusabio) in cell supernatants of THP-1-derived macrophages was quantified using commercial kits following the manufacturer's instructions. OD values were determined at 450 nm with a microplate reader.

2.10 Lipid Peroxidation Measurement

The levels of lipid peroxidation in cells were detected using the lipid peroxide kit (C11-BODIPY 581/591, D3861, Thermo Fisher, USA). After harvesting and washing with 1 × PBS (7.2–7.4), THP-1-derived macrophages were incubated with 1 μM C11-BODIPY in PBS at 37°C for 1 h. Following two additional washes, the cell pellets were suspended in 300 μL PBS for flow cytometry (A00-1-1102, Beckman, Brea, CA, USA) analysis. Cells were gated on FSC-A vs. SSC-A to exclude debris. Then the target cells were identified by gating on PE-A vs. FITC-A. And flow cytometry data were analyzed using FlowJo (v10.8, BD Biosciences, San Jose, CA).

2.11 Methylated RNA Immunoprecipitation Quantitative PCR (MeRIP-qPCR)

To determine PTEN m6A modification, we performed the MeRIP-qPCR assay for PTEN m6A modification using the Imprint® RNA immunoprecipitation kit (RIP, Sigma, St. Louis, MO, USA). Following THP-1-derived macrophage cell lysis, where the lysate consisted of 100 μL of RIP Lysis Buffer, 0.5 μL of protease inhibitor, and 0.25 μL of RNase inhibitor, total RNA was isolated using the RIP Lysis Buffer and subjected to fragmentation. Two centrifuge tubes, designated as IP and Normal IgG, were prepared. Then, 50 μL of magnetic beads and 500 μL of RIP Wash Buffer were added to each tube, allowing the beads to be separated magnetically. After resuspending the beads in RIP Wash Buffer, the target antibody was added to the IP tube, and control IgG was added to the Normal IgG tube. Tubes were rotated for 30 min, separating beads magnetically, washing with 500 μL RIP Wash Buffer, and resuspending in 900 μL RIP Immunoprecipitation Buffer. After clarifying the cell lysate by centrifugation at 13,000 rpm for 10 min at 4°C (H1650R, Xiangyi, Hunan, China), the supernatant was added to each bead-antibody mixture. Then, the lysate supernatant was set aside as the input tube, while another tube of the lysis solution was mixed with loading buffer. The RNA from the IP/Normal IgG/Input sample was purified, and RT-qPCR was performed. The *%Input* was calculated using the formula: $\%Input = 2^{(-\Delta Ct[\text{normalized RIP}])}$.

2.12 Statistical Analysis

In this study, statistical analysis was employed using GraphPad Prism 8.0 software (GraphPad Software, San Diego, CA, USA). Normally distributed data are presented as mean ± standard deviation (SD). The normality of distribution and homogeneity of variance were assessed using the Shapiro-Wilk test and exploratory descriptive statistics, respectively. Group comparisons relied on Student's *t*-test for two groups, and one- or two-way ANOVA for multiple groups, followed by Tukey's test for post hoc comparisons. Image-based quantification was performed by investigators blinded to group allocation. A *p*-value below 0.05 defines statistical significance. All experiments included three independent biological replicates ($n = 3$).

3 Results

3.1 Macrophage Ferroptosis Is Positively Correlated with GA Progression

To investigate the role of macrophage ferroptosis in GA, we established an *in vitro* model by stimulating THP-1-derived macrophages with MSU. Initial analysis revealed that protein levels of the ferroptosis inhibitors GPX4 and SLC7A11 were decreased in the MSU-treated group relative to the Control group (Fig. 1A). IF confirmed reduced co-localization of macrophage marker CD68 and GPX4 in the MSU-treated group compared with the Control group (Fig. 1B). Moreover, Fig. 1C showed that lipid peroxidation was significantly increased in the MSU-treated group. Biochemical assays revealed elevated levels of MDA and Fe^{2+} and reduced levels of GSH and SOD in the MSU-treated group compared to the Control group (Fig. 1D). Activation of ALOX15 can alleviate vascular inflammation and dysfunction [30]. In our work, compared with the Control group, ALOX15 was upregulated in the MSU-treated group (Fig. 1E). The ELISA results showed that the cell supernatant of the MSU-treated group had elevated inflammatory factors (IL-1β, IL-6, and TNF-α) compared to the Control group (Fig. 1F), demonstrating a positive correlation between macrophage-mediated ferroptosis and GA inflammation.

To further examine the relationship between macrophage ferroptosis and GA progression, THP-1 cells were treated with MSU to simulate GA *in vitro* and co-cultured with the hCDs. In this co-culture system, MSU-treated macrophages induced chondrocyte degradation, characterized by decreased Collagen

II and Aggrecan, increased MMP3, and reduced viability of hCDs (Fig. 1G,H). These findings indicate that macrophage ferroptosis induces chondrocyte degradation.

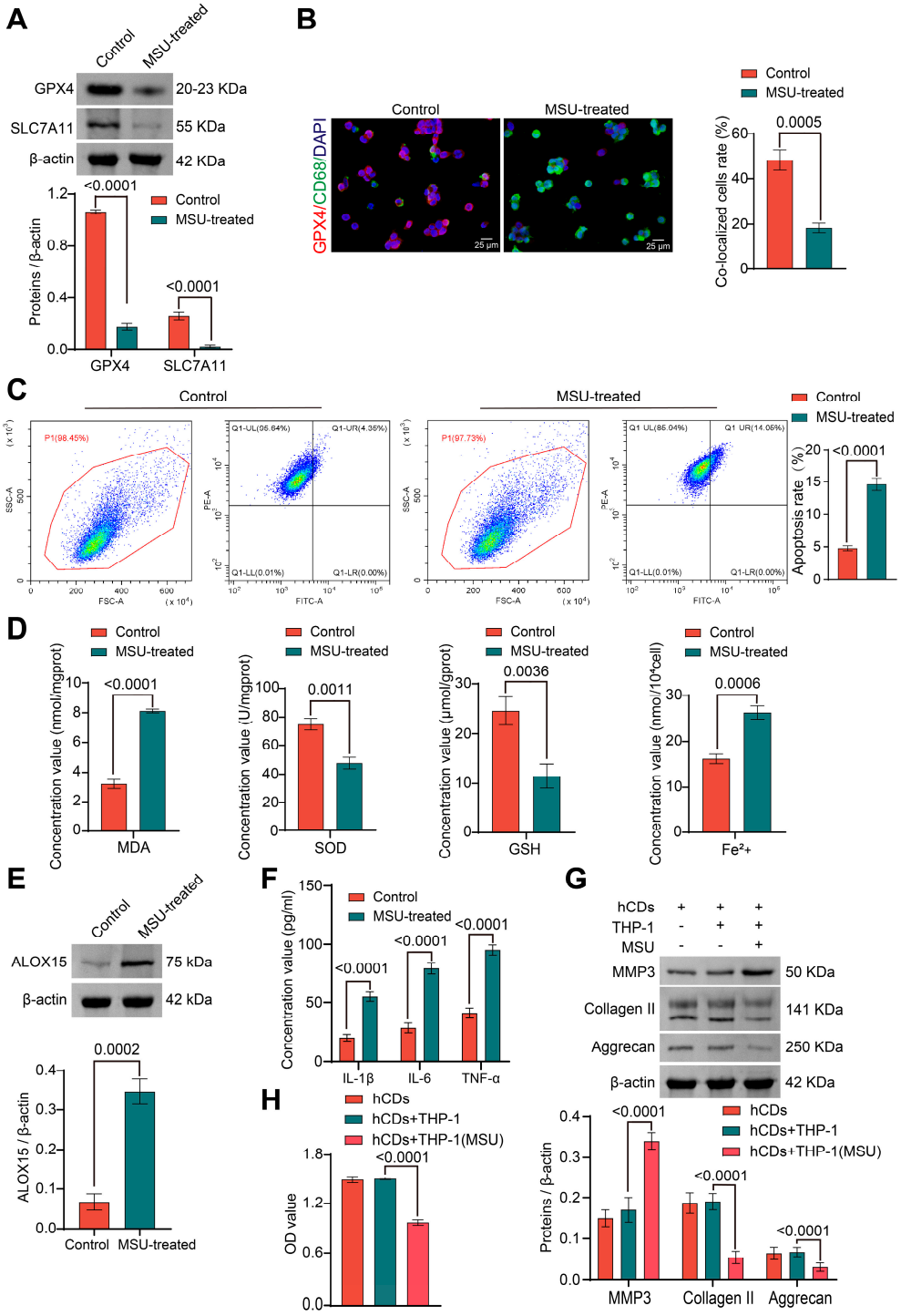

Figure 1: Macrophage ferroptosis is positively correlated with GA progression. (**A**) Representative image of WB detected the levels of GPX4 and SLC7A11. (**B**) Representative image of IF detection of co-localization of GPX4 and CD68; scale bar = 25 μm. (**C**) Representative image of flow cytometry for lipid peroxidation. The flow cytometry gating strategy is as follows: cells were first gated on FSC-A vs. SSC-A to exclude debris. Then the target cells were identified by gating on PE-A vs. FITC-A. (**D**) The concentration of MDA, GSH, SOD, and Fe^{2+} was detected by biochemical assays.

(**E**) Representative image of WB analysis of ALOX15 level. (**F**). Quantification of IL-1β, IL-6, and TNF-α in cell supernatant via ELISA. (**G**) Representative image of WB analysis of MMP3, Collagen II, and Aggrecan levels in hCDs. (**H**) The CCK8 assay was performed to detect the cell viability of hCDs. All data present mean ± standard deviation (SD) (n = 3). Under the assumptions of normal distribution and homogeneity of variance, data were analyzed for significance using one-way analysis of variance (ANOVA) and Tukey's post hoc test.

3.2 PTEN/PI3K/AKT Regulates Macrophage Ferroptosis

The PTEN/PI3K/AKT axis is a key factor in GA development and progression. To clarify the relationship between PTEN/PI3K/AKT and macrophage ferroptosis, we overexpressed PTEN in THP-1 cells within a GA model by transfecting with oe-PTEN. As shown in Fig. 2A, PTEN expression was upregulated in the MSU-treated+oe-PTEN group compared with the MSU-treated+oe-NC group. As expected, PTEN overexpression effectively inhibited the activation of the PI3K/AKT pathway, evidenced by significantly reduced ratios of p-PI3K/PI3K and p-AKT/AKT (Fig. 2B). These results indicate that PTEN overexpression effectively inhibited the activation of the PI3K/AKT pathway in the GA model. Fig. 2C,D showed that PTEN overexpression upregulated GPX4 and SLC7A11, and enhanced the co-localization of GPX4 and CD68. Additionally, PTEN overexpression inhibited lipid peroxidation, decreased Fe^{2+} and MDA levels, and upregulated antioxidant markers, including GSH and SOD (Fig. 2E,F). PTEN overexpression decreased MSU-induced ALOX15 protein level (Fig. 2G). Fig. 2H showed that PTEN overexpression downregulated inflammatory factors (IL-1β, IL-6, and TNF-α) levels. Collectively, these data demonstrate that PTEN activation suppresses macrophage ferroptosis and inflammation by inhibiting the PI3K/AKT pathway.

Subsequently, PTEN-overexpressing THP-1 cells were co-cultured with hCDs in an MSU-induced GA model. Fig. 2I,J showed that PTEN overexpression promoted Collagen II, Aggrecan, and viability of hCDs, but inhibited MMP3, implying that PTEN overexpression inhibited chondrocyte degradation, which was related to macrophage ferroptosis.

Following PTEN knockdown in THP-1-derived macrophages, cells were treated with 2 μM ferroptosis inhibitor Fer-1 for 24 h [8]. WB analysis revealed that Fer-1 treatment downregulated ALOX15 and upregulated the key ferroptosis inhibitors GPX4 and SLC7A11, which reversed the effect of sh-PTEN (Fig. S1A). Correspondingly, at the biochemical level, Fer-1 treatment reduced MDA levels and elevated GSH and SOD levels in macrophages and reversed the effect of sh-PTEN (Fig. S1B). Collectively, these findings suggest that Fer-1 inhibits ferroptosis induced by the PTEN pathway in macrophages.

3.3 PTEN Is Highly m6A-Modified in Macrophages Treated with MSU

M6A is the most common RNA modification in mammals and participates in macrophage activation during immune response and the inflammatory process [31]. To investigate the effect of m6A modification in PTEN on ferroptosis of GA-related macrophages, we first examined the global m6A levels. As shown in Fig. 3A, the total m6A level was significantly increased in MSU-treated macrophages compared with controls. MeRIP-qPCR confirmed that PTEN mRNA exhibited increased m6A modification in the MSU-treated group compared to the Control group (Fig. 3B). Consistently, both the mRNA and protein levels of the key m6A methyltransferase METTL3 were also upregulated upon MSU treatment (Fig. 3C,D). Together, these data confirmed that PTEN m6A and METTL3 levels are increased in MSU-treated macrophages.

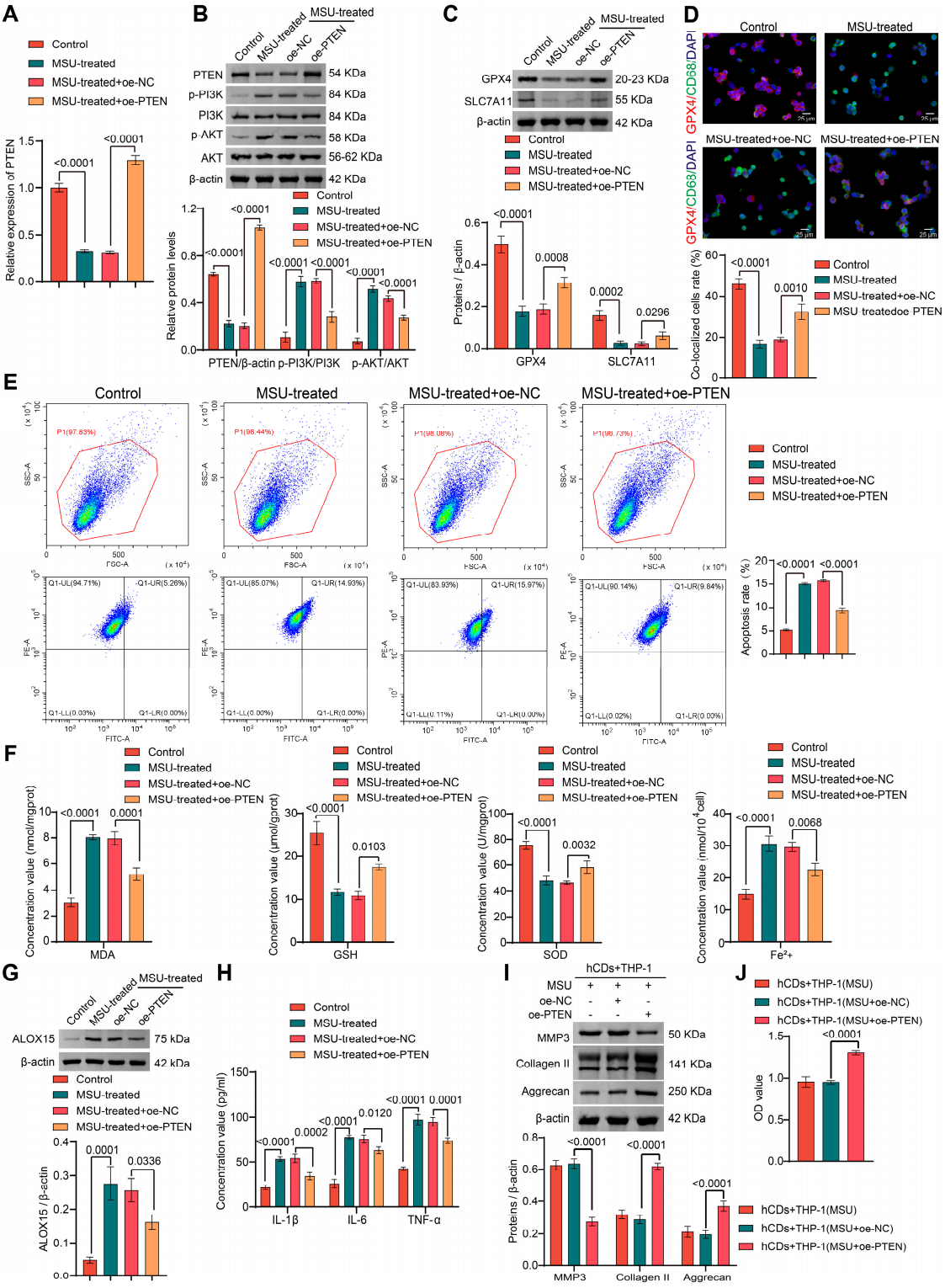

Figure 2: PTEN/PI3K/AKT regulates macrophage ferroptosis. (**A**) RT-qPCR detection of PTEN mRNA expression. (**B**) Representative image of WB detection of PTEN, p-PI3K/PI3K, p-AKT/AKT. (**C**) Representative image of WB detection of GPX4 and SLC7A11. (**D**) Representative image of IF detected the co-localization of GPX4 and CD68; scale bar = 25 μm. (**E**) Flow cytometry detection of lipid peroxidation. (**F**) Biochemical kits to detect MDA, GSH, SOD, and Fe^{2+} levels. The flow cytometry gating strategy is as follows: cells were first gated on FSC-A vs. SSC-A to exclude debris.

Then the target cells were identified by gating on PE-A vs. FITC-A. (**G**) Representative image of WB analysis of ALOX15 level. (**H**) ELISA detection of the concentration of IL-1β, IL-6, and TNF-α in cell supernatant. (**I**) Representative image of WB detection of MMP3, Collagen II, and Aggrecan levels in hCDs. (**J**) CCK8 assay for hCD viability. All data present mean ± standard deviation (SD) (n = 3). The data were analyzed for significance using one-way ANOVA and Tukey's post hoc test, under the premise that the data satisfied the assumptions of normal distribution and homogeneity of variance.

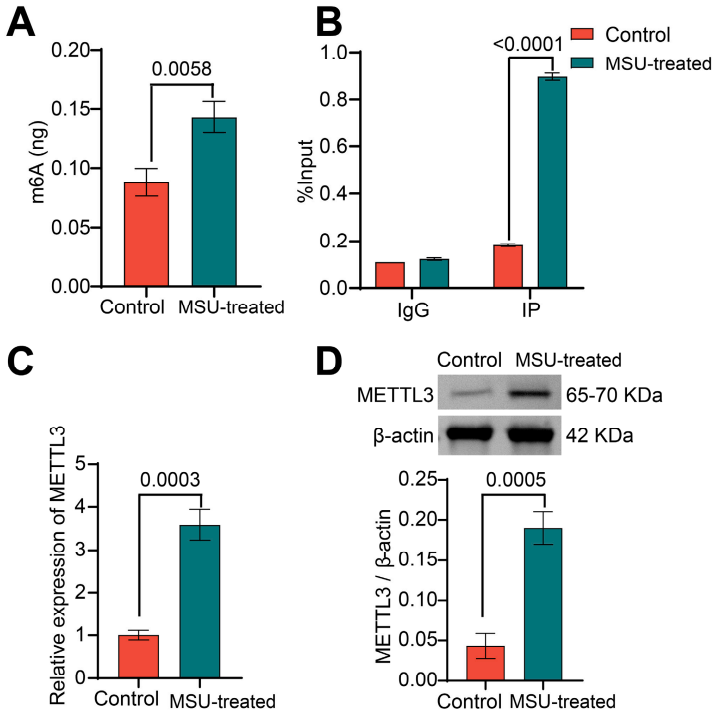

Figure 3: PTEN is highly modified by m6A in MSU-treated macrophages. (**A**) The kit detected the total m6A level. (**B**) MeRIP-qPCR detection of PTEN m6A level. (**C**) Detection of METTL3 by RT-qPCR. (**D**) Representative image of WB analysis of METTL3 level. All data present mean ± standard deviation (SD) (n = 3). Under the assumptions of normal distribution and homogeneity of variance, data were analyzed for significance using one-way analysis of variance (ANOVA) and Tukey's post hoc test.

3.4 METTL3 Regulates PTEN Expression via m6A Modification

Then, we established METTL3-overexpressing and METTL3-knockdown THP-1 cell lines by transfecting oe-METTL3 and sh-METTL3. RT-qPCR and WB results demonstrated that the sh-METTL3 group had increased PTEN expression and decreased METTL3 expression compared to the sh-NC group; conversely, the oe-METTL3 group exhibited decreased PTEN expression and increased METTL3 expression compared to the oe-NC group (Fig. 4A,B). These data indicate that METTL3 negatively regulates PTEN expression. MeRIP-qPCR analysis confirmed that METTL3 overexpression increased the PTEN m6A modification level (Fig. 4C). RNA stability assays using actinomycin D showed that METTL3 overexpression accelerated PTEN mRNA decay, while METTL3 knockdown stabilized it (Fig. 4D). YTHDF2 is an m6A reader protein and binds to PTEN mRNA, as demonstrated by RIP-qPCR (Fig. 4E). Furthermore, YTHDF2 knockdown reversed the increase in PTEN expression induced by METTL3 overexpression (Fig. 4F). These findings indicate that METTL3 regulates PTEN expression via m6A modification.

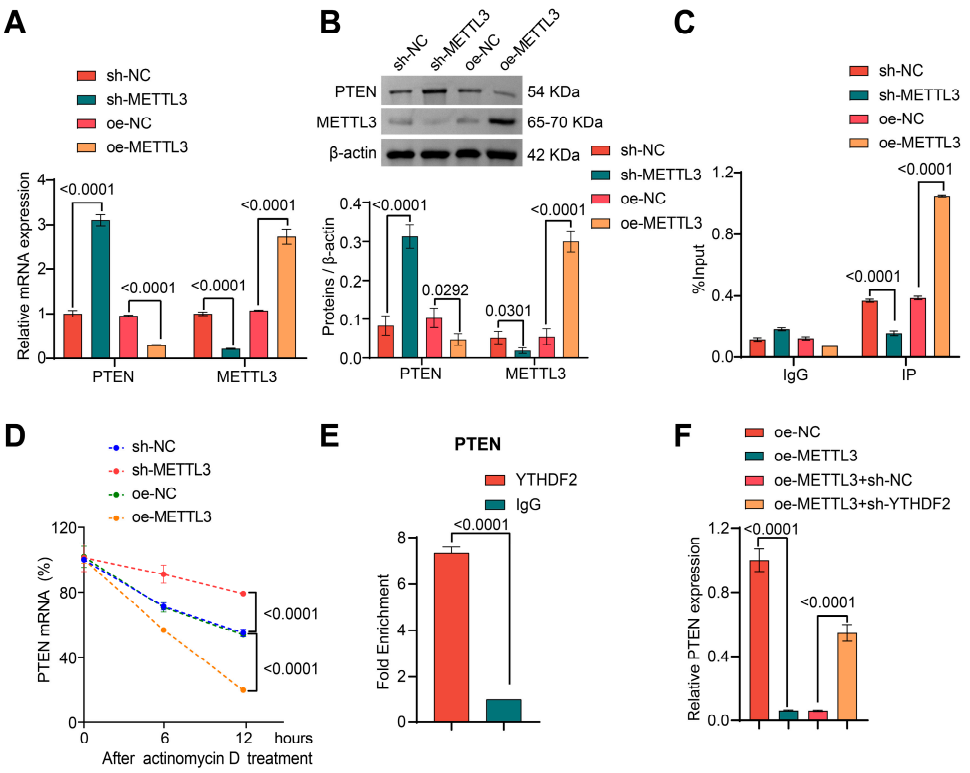

Figure 4: METTL3 regulates PTEN expression through m6A modification. (**A**,**B**) RT-qPCR and a representative image of WB detected the levels of PTEN and METTL3 in THP-1 cells. (**C**) MeRIP-qPCR detection of PTEN m6A level. (**D**) RNA stability assay detection of PTEN mRNA at 0, 6, and 12 h after actinomycin D treatment. (**E**) RIP-qPCR assay analysis of the binding of YTHDF2 to PTEN. (**F**) RT-qPCR detection of PTEN mRNA. All data present mean ± standard deviation (SD) (n = 3). Under the assumptions of normal distribution and homogeneity of variance, data were analyzed for significance using one-way analysis of variance (ANOVA) and Tukey's post hoc test.

3.5 METTL3 Regulates Macrophage Ferroptosis via PTEN

Next, we knocked down both METTL3 and PTEN (sh-METTL3+sh-PTEN). RT-qPCR analysis also confirmed that METTL3 negatively regulated PTEN mRNA expression (Fig. 5A). WB analysis showed that PTEN knockdown increased the p-PI3K/PI3K and p-AKT/AKT ratios, while decreasing the expression of PTEN, GPX4, and SLC7A11. Conversely, concurrent METTL3 knockdown reversed all these effects induced by PTEN knockdown (Fig. 5B,C). These results showed that METTL3 promoted PTEN expression and inhibited the phosphorylation of PI3K and AKT. IF staining demonstrated that the co-localization of GPX4 and CD68 was inhibited in sh-PTEN macrophages. However, dual knockdown of METTL3 and PTEN reversed the effect of sh-PTEN (Fig. 5D). Flow cytometry results showed that lipid peroxidation level in the sh-METTL3+sh-PTEN group was lower than in the sh-PTEN group (Fig. 5E). Furthermore, PTEN knockdown decreased the levels of GSH and SOD in cell culture media, while increasing the levels of MDA and Fe^{2+}. However, the effect of PTEN knockdown was reversed by concurrent METTL3 knockdown (Fig. 5F). Similarly, PTEN knockdown upregulated the expression of ALOX15, which was also reversed by the dual knockdown of PTEN and METTL3 (Fig. 5G). ELISA assays showed upregulated levels of IL-1β, IL-6, and TNF-α in the sh-PTEN group in comparison with the sh-NC group. However, dual knockdown of METTL3 and PTEN attenuated these pro-inflammatory effects, indicating that METTL3 knockdown counteracts the pro-inflammatory effects mediated by PTEN knockdown (Fig. 5H). In a co-culture system

of hCDs under MSU stimulation for 12 h. WB analysis revealed that PTEN knockdown upregulated MMP3 and downregulated Collagen II and Aggrecan expression compared to controls. These effects were rescued by the concurrent knockdown of METTL3 (Fig. 5I). CCK8 assays demonstrated that sh-PTEN inhibited the viability of hCDs, an effect that was reversed by METTL3 knockdown (Fig. 5J). Taken together, these findings demonstrate that METTL3 regulates macrophage ferroptosis and chondrocyte degeneration through the PTEN/PI3K/AKT pathway.

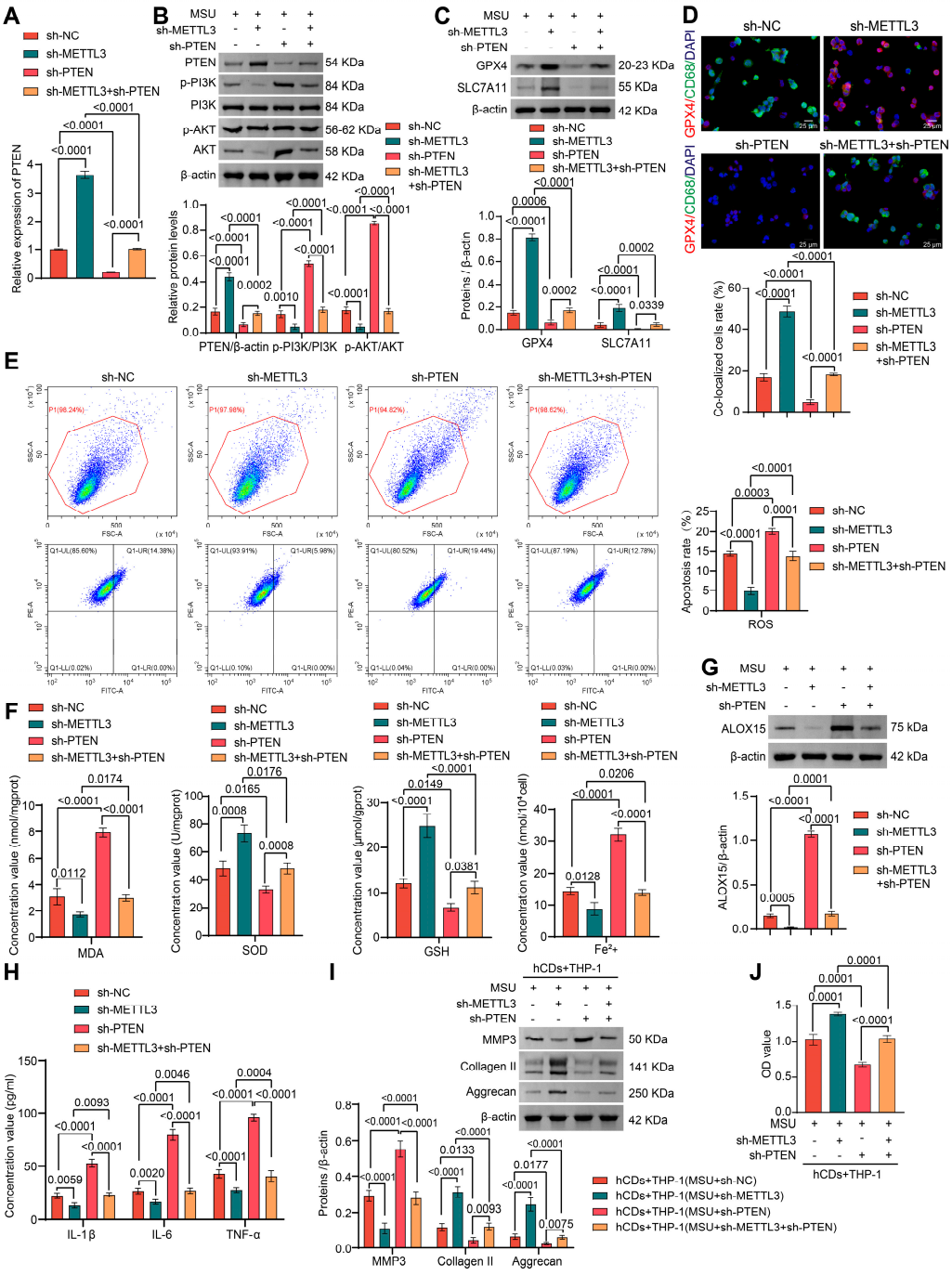

Figure 5: METTL3 mediates macrophage ferroptosis by regulating PTEN. (**A**) RT-qPCR detection of PTEN mRNA expression. (**B**) Representative image of WB detection of PTEN, p-PI3K/PI3K, p-AKT/AKT level in MSU-treated THP-1 cells.

(**C**) Representative image of WB detection of GPX4 and SLC7A11 levels in MSU-treated THP-1 cells. (**D**) Representative image of IF analysis of GPX4 and CD68 co-localization in macrophages; scale bar = 25 μm. (**E**) Representative image of Flow cytometry detection of lipid peroxidation. The flow cytometry gating strategy is as follows: cells were first gated on FSC-A vs. SSC-A to exclude debris. Then the target cells were identified by gating on PE-A vs. FITC-A. (**F**) Biochemical assays to detect MDA, GSH, SOD, and Fe^{2+} levels. (**G**) Representative image of WB assay analysis of ALOX15 level. (**H**) ELISA was used to detect the levels of IL-1β, IL-6, and TNF-α in cell supernatant. (**I**) Representative image of WB determined the levels of MMP3, Collagen II, and Aggrecan in hCDs. (**J**) CCK8 assay for hCD viability. All data present mean ± standard deviation (SD) (n = 3). Under the assumptions of normal distribution and homogeneity of variance, data were analyzed for significance using one-way analysis of variance (ANOVA) and Tukey's post hoc test.

4 Discussion

GA is characterized by an inflammatory reaction triggered by MSU crystals, which often leads to serious complications such as joint deformity and chronic kidney disease [32]. Recent studies have revealed that multiple pathogenic mechanisms in GA, including cartilage extracellular matrix (CEM) degradation [33], and NF-κB signaling-mediated activation of fibroblast-like synoviocytes (FLS) and inflammation [34]. However, the role of m6A modification and macrophage ferroptosis in GA remains poorly understood. Our research revealed that METTL3-mediated m6A modification reduces PTEN mRNA stability and gene expression, thereby activating the PI3K/AKT pathway. This inhibition promotes macrophage ferroptosis and amplifies inflammatory signaling, exacerbating pro-inflammatory cytokine release, leading to chondrocyte degeneration and the progression of GA. This study offers a fresh perspective on the underlying mechanisms of inflammation and chondrocyte degeneration in GA.

m6A modification, a prevalent epigenetic mark in mRNA, is a key component of the epigenetic regulatory network [35]. The methyltransferase METTL3 catalyzes the deposition of m6A [36]. Although existing studies have revealed that METTL3 has been widely implicated in regulating immune responses and cell death in various diseases, including cancer and inflammatory bowel disease, its specific role in the macrophage-driven pathology of GA remains unexplored [37–39]. In polycystic ovary syndrome, METTL3 knockdown increases GPX4 levels through m6A modification, thereby inhibiting ferroptosis and fibrosis [37]. In inflammatory bowel disease, the progression of *Bacteroides fragilis* toxin represses METTL3-mediated m6A modification in macrophages, thereby exacerbating the pathogenesis [38]. In lung adenocarcinoma, METTL3 promotes cell proliferation and inhibits ferroptosis by stabilizing SLC7A11 m6A modification [39]. Yin et al. reported that METTL3-deficient mice showed enhanced accumulation of M1/M2-like tumor-associated macrophages and regulatory T cells within tumors [40]. Notably, whether METTL3-mediated m6A modification regulates macrophage ferroptosis and GA pathology remains unclear. Our study addresses this gap and indicates that in MSU-stimulated macrophages, upregulated METTL3 increased the m6A modification of PTEN mRNA, leading to its destabilization and reduced expression. This downregulation of PTEN leads to changes in metabolism and an imbalance in the antioxidant system, which promotes ferroptosis in macrophages.

PTEN is identified as a tumor suppressor and a pivotal regulator of the PI3K/AKT pathway, which mediates cell survival, proliferation, differentiation, and metabolism [41]. Previous studies demonstrated that the PTEN/PI3K/AKT axis promotes chondrocyte proliferation and inhibits apoptosis, mediated by miR-132 and miR-130a [42,43]. Our study reveals a novel regulatory axis in macrophages. METTL3-mediated m6A modification induces macrophage ferroptosis by reducing PTEN levels and inhibiting the PTEN-dependent PI3K/AKT pathway. Specifically, METTL3 knockdown diminished m6A modification on PTEN mRNA, leading to increased PTEN expression, suppressed the PI3K/AKT pathway, increased antioxidant markers

GSH and SOD, and reduced macrophage ferroptosis. Collagen II and Aggrecan maintain cartilage integrity and function, whereas MMP3 degrades the cartilage extracellular matrix [44]. Generally, activation of the PI3K/Akt pathway has been reported to inhibit ferroptosis in chondrocytes [45]. In contrast, other studies have indicated that PI3K/Akt activation promotes ferroptosis in macrophages [46]. Consistently, our study indicated that PTEN downregulation activates the PI3K/AKT pathway to promote ferroptosis in macrophages.

Our study provides the first evidence linking the METTL3/PTEN/PI3K/AKT axis to macrophage ferroptosis in GA. We demonstrate that MSU crystals upregulate METTL3 to drive this pathway. This METTL3/PTEN/m6A/ferroptosis axis contributes to chondrocyte degeneration and disease progression in GA. This inhibition of PTEN triggers activation of the PI3K/AKT pathway. We propose that in the inflammatory environment of GA, the specific PI3K/AKT activation undergoes metabolic reprogramming (such as increased dependence on iron and lipids), thereby making cells more sensitive to ferroptosis, ultimately contributing to chondrocyte degeneration and disease progression. In this study, we construct the METTL3-m6A-PTEN-PI3K/AKT-ferroptosis signaling axis to explain this causal chain. The m6A modification mediated by METTL3 may not only directly affect the stability of PTEN mRNA but could also exert indirect regulatory effects by modulating its upstream regulators. We propose this possibility as one of the directions for future mechanistic research.

Nonetheless, this study has certain limitations. Firstly, we established an *in vitro* model of GA inflammation by stimulating THP-1 cells with MSU and PMA, and then co-culturing them with hCDs. The model of primary or synovial macrophages is valuable for further mechanistic studies. More importantly, the model used in this study replicates the complex dynamic interactions among cells *in vivo*. Due to the limitations of our laboratory's facilities and resources, future validation in other human chondrocyte cell lines or macrophage-specific METTL3-knockout mice is required. Despite this limitation, we believe our current work provides the first evidence elucidating the role of the METTL3/PTEN m6A axis in regulating macrophage ferroptosis in GA, establishing a foundational mechanistic framework. Secondly, joint fluid and synovial tissue samples from GA patients should be supplemented to detect the correlation among METTL3 expression, PTEN mRNA m6A modification levels, and ferroptosis markers. However, we did not acquire well-matched clinical samples in the present study due to constraints in experimental conditions and tissue source availability. Thirdly, while we show that METTL3 regulates PTEN via m6A, the specific modification sites on PTEN mRNA, which could be mapped by techniques like MeRIP-seq, remain unidentified. Consequently, direct evidence from rescue experiments using m6A site-deficient PTEN mutants remains to be explored. Finally, the development of METTL3 inhibitors or macrophage-targeted ones may represent a safer therapeutic strategy. Currently, the METTL3/PTEN small molecule inhibitors (such as STM2457) and METTL3 inhibitors (such as STC-15) have moved from concept to clinical application, providing a realistic basis for treating diseases, including cancer [47,48]. PTEN inhibitors VO-OHpic may serve as an intervention treatment method [49]. Building on these, future research should explore macrophage-specific delivery of METTL3 inhibitors to achieve a more precise therapeutic outcome, for instance, through nanoparticle encapsulation or antibody-drug conjugation technologies. Alternatively, strategies could be developed to modulate macrophage functional states specifically.

5 Conclusion

Our findings delineate a pathogenic signaling axis in GA: METTL3-mediated m6A modification of PTEN mRNA suppresses PTEN expression, thereby relieving its inhibition of the PI3K/AKT pathway. This cascade ultimately promotes ferroptosis in macrophage and chondrocyte degeneration. Collectively, these

findings show that the METTL3/PTEN axis may be a mechanistically plausible and therapeutically relevant target for the treatment of gouty arthritis.

Acknowledgement: None.

Funding Statement: This study was sponsored by the Science Foundation of Hunan Aerospace Hospital, 2023YJ04.

Author Contributions: The authors confirm contribution to the paper as follows: conceptualization, Xingchang Fu; methodology, Xingchang Fu; formal analysis, Gang Yang and Xiongwu Long; data curation, Gang Yang and Xiongwu Long; writing—original draft preparation, Gang Yang and Xiongwu Long; writing—review and editing, Xingchang Fu; visualization, Gang Yang and Xiongwu Long; project administration, Xingchang Fu. All authors reviewed and approved the final version of the manuscript.

Availability of Data and Materials: The data that support the findings of this study are available from the corresponding author [Xingchang Fu] upon reasonable request.

Ethics Approval: Not applicable.

Conflicts of Interest: The authors declare no conflicts of interest.

Supplementary Materials: The supplementary material is available online at https://www.techscience.com/doi/10.32604/biocell.2026.075362/s1. Figure S1: PTEN/PI3K/AKT regulates macrophage ferroptosis. (**A**) Representative image of WB analysis of GPX4, SLC7A11, and ALOX15. (**B**) Biochemical kits to detect MDA, SOD, and GSH levels. All data present mean ± standard deviation (SD) (n = 3). Under the assumptions of normal distribution and homogeneity of variance, data were analyzed for significance using one-way analysis of variance (ANOVA) and Tukey's post hoc test. Supplementary File S1: Cell line testing reports. Supplementary File S2: Uncropped WB bands.

References

1. Tao H, Mo Y, Liu W, Wang H. A review on gout: Looking back and looking ahead. Int Immunopharmacol. 2023;117:109977. [CrossRef].
2. So AK, Martinon F. Inflammation in gout: Mechanisms and therapeutic targets. Nat Rev Rheumatol. 2017;13(11):639–47. [CrossRef].
3. Ehirchiou D, Bernabei I, Pandian VD, Nasi S, Chobaz V, Castelblanco M, et al. The integrin CD11b inhibits MSU-induced NLRP3 inflammasome activation in macrophages and protects mice against MSU-induced joint inflammation. Arthritis Res Ther. 2024;26(1):119. [CrossRef].
4. Dalbeth N, Choi HK, Joosten LAB, Khanna PP, Matsuo H, Perez-Ruiz F, et al. Gout (primer). Nat Rev Dis Primers. 2019;5(1):69. [CrossRef].
5. Yao TK, Lee RP, Wu WT, Chen IH, Yu TC, Yeh KT. Advances in gouty arthritis management: Integration of established therapies, emerging treatments, and lifestyle interventions. Int J Mol Sci. 2024;25(19):10853. [CrossRef].
6. Liu J, Zhong W, Wang R, Wang P, Tong G, Chai M, et al. macrophage ferroptotic resistance is required for the progression of infantile hemangioma. J Am Heart Assoc. 2025;14(1):e034261. [CrossRef].
7. Zhao H, Tang C, Wang M, Zhao H, Zhu Y. Ferroptosis as an emerging target in rheumatoid arthritis. Front Immunol. 2023;14:1260839. [CrossRef].
8. Liu Y, Luo X, Chen Y, Dang J, Zeng D, Guo X, et al. Heterogeneous ferroptosis susceptibility of macrophages caused by focal iron overload exacerbates rheumatoid arthritis. Redox Biol. 2024;69:103008. [CrossRef].
9. Feng Z, Meng F, Huo F, Zhu Y, Qin Y, Gui Y, et al. Inhibition of ferroptosis rescues M2 macrophages and alleviates arthritis by suppressing the HMGB1/TLR4/STAT3 axis in M1 macrophages. Redox Biol. 2024;75:103255. [CrossRef].
10. Chen C, Wang J, Guo Y, Li M, Yang K, Liu Y, et al. Monosodium urate crystal-induced pyroptotic cell death in neutrophil and macrophage facilitates the pathological progress of gout. Small. 2024;20(23):e2308749. [CrossRef].

11. Zhao X, Li M, Lu Y, Wang M, Xiao J, Xie Q, et al. Sirt1 inhibits macrophage polarization and inflammation in gouty arthritis by inhibiting the MAPK/NF-κB/AP-1 pathway and activating the Nrf2/HO-1 pathway. Inflamm Res. 2024;73(7):1173–84. [CrossRef].
12. Givian A, Azizan A, Jamshidi A, Mahmoudi M, Farhadi E. Iron metabolism in rheumatic diseases. J Transl Autoimmun. 2025;10:100267. [CrossRef].
13. Zhang S, Li D, Fan M, Yuan J, Xie C, Yuan H, et al. Mechanism of reactive oxygen species-guided immune responses in gouty arthritis and potential therapeutic targets. Biomolecules. 2024;14(8):978. [CrossRef].
14. Fatima T, McKinney C, Major TJ, Stamp LK, Dalbeth N, Iverson C, et al. The relationship between ferritin and urate levels and risk of gout. Arthritis Res Ther. 2018;20(1):179. [CrossRef].
15. Li Y, Huang C, Xie Y, Liu W, Wei M, Li S, et al. JUN and ATF3 in Gout: Ferroptosis-related potential diagnostic biomarkers. Heliyon. 2024;10(22):e39957. [CrossRef].
16. Reifenberger J, Wolter M, Boström J, Büschges R, Schulte KW, Megahed M, et al. Allelic losses on chromosome arm 10q and mutation of the PTEN (MMAC1) tumour suppressor gene in primary and metastatic malignant melanomas. Virchows Arch. 2000;436(5):487–93. [CrossRef].
17. Zhou P, Meng X, Nie Z, Wang H, Wang K, Du A, et al. PTEN: An emerging target in rheumatoid arthritis? Cell Commun Signal. 2024;22(1):246. [CrossRef].
18. Kumar M, Bansal N. Implications of phosphoinositide 3-kinase-Akt (PI3K-Akt) pathway in the pathogenesis of Alzheimer's disease. Mol Neurobiol. 2022;59(1):354–85. [CrossRef].
19. Su Y, Wang B, Huang J, Huang M, Lin T. YTHDC1 positively regulates PTEN expression and plays a critical role in cisplatin resistance of bladder cancer. Cell Prolif. 2023;56(7):e13404. [CrossRef].
20. Wang Q, Shen J, Luo S, Yuan Z, Wei S, Li Q, et al. METTL3-m6A methylation inhibits the proliferation and viability of type II alveolar epithelial cells in acute lung injury by enhancing the stability and translation efficiency of Pten mRNA. Respir Res. 2024;25(1):276. [CrossRef].
21. Jiang Y, Liu H, Shi R, Hao Y, Zhang J, Xin W, et al. Methyltransferase-Like 3-Mediated N6-Methyladenosine RNA Methylation Regulates Hypoxia-Induced Pulmonary Arterial Smooth Muscle Cell Pyroptosis by Targeting PTEN. J Am Heart Assoc. 2024;13(19):e034470. [CrossRef].
22. Wang F, Bai J, Zhang X, Wang D, Zhang X, Xue J, et al. METTL3/YTHDF2 m6A axis mediates the progression of diabetic nephropathy through epigenetically suppressing PINK1 and mitophagy. J Diabetes Investig. 2024;15(3):288–99. [CrossRef].
23. Guo M, Yan R, Ji Q, Yao H, Sun M, Duan L, et al. IFN regulatory Factor-1 induced macrophage pyroptosis by modulating m6A modification of circ_0029589 in patients with acute coronary syndrome. Int Immunopharmacol. 2020;86:106800. [CrossRef].
24. Qi L, Wang Y, Hu H, Li P, Hu H, Li Y, et al. m(6)A methyltransferase METTL3 participated in sympathetic neural remodeling post-MI via the TRAF6/NF-κB pathway and ROS production. J Mol Cell Cardiol. 2022;170:87–99. [CrossRef].
25. Li X, Jiang Y, Sun X, Wu Y, Chen Z. METTL3 is required for maintaining β-cell function. Metabolism. 2021;116:154702. [CrossRef].
26. Wu B, Li D, Wang Y, Pan T, Xu J, Li L. The m6A methyltransferase METTL3 affects ferroptosis in non-small cell lung cancer by regulating the PTEN/PI3K/AKT pathway. Discov Oncol. 2025;16(1):559. [CrossRef].
27. Luo X, Wang Y, Zhu X, Chen Y, Xu B, Bai X, et al. MCL attenuates atherosclerosis by suppressing macrophage ferroptosis via targeting KEAP1/NRF2 interaction. Redox Biol. 2024;69:102987. [CrossRef].
28. Meng Q, Meng W, Bian H, Zheng F, Gu H, Zuo R, et al. Total glucosides of paeony protects THP-1 macrophages against monosodium urate-induced inflammation via MALAT1/miR-876-5p/NLRP3 signaling cascade in gouty arthritis. Biomed Pharmacother. 2021;138:111413. [CrossRef].
29. Fu S, Du H, Ling X, Wang H, Chen J, Zhang H, et al. Suppressing chondrocyte cuproptosis by syringaresinol-4-O-β-d-glucoside alleviates gouty arthritis. Front Pharmacol. 2025;16:1565422. [CrossRef].
30. Yan W, Cui X, Guo T, Liu N, Wang Z, Sun Y, et al. ALOX15 aggravates metabolic dysfunction-associated steatotic liver disease in mice with type 2 diabetes via activating the PPARγ/CD36 axis. Antioxid Redox Signal. 2025;43(1–3):37–55. [CrossRef].

31. Wan L, Liu J, Huang C, Zhu Z, Wang K, Sun G, et al. Comprehensive analysis and functional characteristics of differential expression of n6-methyladenosine methylation modification in the whole transcriptome of rheumatoid arthritis. Mediators Inflamm. 2022;2022:4766992. [CrossRef].
32. Tang D, Jiang Y, Ling G, Zhang J, Xie J. Case report: Gouty renal abscess and gouty sacroiliitis associated with genetic variants of a young woman. Front Med. 2025;12:1509018. [CrossRef].
33. Sang W, Xue S, Jiang Y, Lu H, Zhu L, Wang C, et al. METTL3 involves the progression of osteoarthritis probably by affecting ECM degradation and regulating the inflammatory response. Life Sci. 2021;278:119528. [CrossRef].
34. Shi W, Zheng Y, Luo S, Li X, Zhang Y, Meng X, et al. METTL3 promotes activation and inflammation of FLSs through the NF-κB signaling pathway in rheumatoid arthritis. Front Med. 2021;8:607585. [CrossRef].
35. Poh HX, Mirza AH, Pickering BF, Jaffrey SR. Alternative splicing of METTL3 explains apparently METTL3-independent m6A modifications in mRNA. PLoS Biol. 2022;20(7):e3001683. [CrossRef].
36. Mi H, Wang M, Chang Y. The potential impact of polymorphisms in METTL3 gene on knee osteoarthritis susceptibility. Heliyon. 2024;10(7):e28035. [CrossRef].
37. Shen C, Jiang Y, Lin J, Guo Q, Fang D. METTL3 silencing inhibits ferroptosis to suppress ovarian fibrosis in PCOS by upregulating m6A modification of GPX4. J Mol Histol. 2024;55(6):1163–75. [CrossRef].
38. Yan Y, Tian L, Zhao Y, Xuan B, Xu X, Ding J, et al. Bacteroides fragilis toxin suppresses METTL3-mediated m6A modification in macrophage to promote inflammatory bowel disease. J Crohns Colitis. 2025;19(3):jjae179. [CrossRef].
39. Xu Y, Lv D, Yan C, Su H, Zhang X, Shi Y, et al. METTL3 promotes lung adenocarcinoma tumor growth and inhibits ferroptosis by stabilizing SLC7A11 m(6)A modification. Cancer Cell Int. 2022;22(1):11. [CrossRef].
40. Yin H, Zhang X, Yang P, Zhang X, Peng Y, Li D, et al. RNA m6A methylation orchestrates cancer growth and metastasis via macrophage reprogramming. Nat Commun. 2021;12(1):1394. [CrossRef].
41. Shan T, Liu J, Xu Z, Wang Y. Roles of phosphatase and tensin homolog in skeletal muscle. J Cell Physiol. 2019;234(4):3192–6. [CrossRef].
42. Zhang W, Hu C, Zhang C, Luo C, Zhong B, Yu X. MiRNA-132 regulates the development of osteoarthritis in correlation with the modulation of PTEN/PI3K/AKT signaling. BMC Geriatr. 2021;21(1):175. [CrossRef].
43. Zhang Y, Xu S, Huang E, Zhou H, Li B, Shao C, et al. MicroRNA-130a regulates chondrocyte proliferation and alleviates osteoarthritis through PTEN/PI3K/Akt signaling pathway. Int J Mol Med. 2018;41(6):3699–708. [CrossRef].
44. Yang W, Hu L, Tian Y, Yang Y, Guo W, Xiao K, et al. WTAP improves chondrocyte loss and dysfunctions to ameliorate osteoarthritis through mediating the mA methylation and mRNA stability of IL-33. Int J Biol Macromol. 2025;306(Pt 3):141330. [CrossRef].
45. Zhao ZM, Ding JM, Li Y, Wang DC, Kuang MJ. Human umbilical cord mesenchymal stem cell-derived exosomes promote osteogenesis in glucocorticoid-induced osteoporosis through PI3K/AKT signaling pathway-mediated ferroptosis inhibition. Stem Cells Transl Med. 2025;14(3):szae096. [CrossRef].
46. Zhan M, Liu D, Yao L, Wang W, Zhang R, Xu Y, et al. Gas6/AXL alleviates hepatic ischemia/reperfusion injury by inhibiting ferroptosis via the PI3K/AKT pathway. Transplantation. 2024;108(11):e357–69. [CrossRef].
47. Li M, Ye J, Xia Y, Li M, Li G, Hu X, et al. METTL3 mediates chemoresistance by enhancing AML homing and engraftment via ITGA4. Leukemia. 2022;36(11):2586–95. [CrossRef].
48. Tang H, Zhang R, Zhang A. Small-molecule inhibitors targeting RNA m(6)A modifiers for cancer therapeutics: Latest advances and future perspectives. J Med Chem. 2025;68(17):18114–42. [CrossRef].
49. Lv M, Xu Q, Zhang B, Yang Z, Xie J, Guo J, et al. Imperatorin induces autophagy and G0/G1 phase arrest via PTEN-PI3K-AKT-mTOR/p21 signaling pathway in human osteosarcoma cells *in vitro* and *in vivo*. Cancer Cell Int. 2021;21(1):689. [CrossRef].